SCIENTIFIC ARTICLE

Damage in a Distal Radius Fracture Model Treated With Locked Volar Plating After Simulated Postoperative Loading

Christina Salas, PhD,*†‡ Justin A. Brantley, MS,*‡ James Clark, MD,* Mahmoud Reda Taha, PhD,§ Deana M. Mercer, MD,* Orrin B. Myers, PhD‖

Purpose "Damage" is an engineering term defining a period between a state of material perfection and the onset of crack initiation. Clinically, it is a loss of fixation due to microstructural breakdown, indirectly measured as a reduction of stiffness of the bone-implant construct, normalized by the cross-sectional area and length of the bone. The purpose of this study was to characterize damage in a cadaver model of extra-articular distal radius fracture with dorsal comminution treated using 2-column volar distal radius plates.

Methods Ten matched distal radii were randomly divided into 2 groups: group I specimens were treated with a volar distal radius plate with an independent, 2-tiered scaffold design; group II specimens (contralateral limbs) were treated with a volar plate with a single-head design for enhanced ulnar buttressing. Specimens were cyclically loaded to simulate a 6-month postoperative load-bearing period. We report damage after a defined protocol of cyclical loading and load to failure simulating a fall on an outstretched hand.

Results Group II specimens experienced more damage under cyclic loading conditions than group I specimens. Group I specimens were stiffer than group II specimens under load-to-failure conditions. Ultimate force at failure in group I and group II specimens was not different. Specimens failed by plate bending (group I, n = 6/10; group II, n = 2/10) and fracture of the lunate facet (group I, n = 4/10; group II, n = 8/10).

Conclusions Group I specimens had less screw cutout at the lunate facet than group II specimens under cyclic loading as indicated by lower damage measures and fewer facet fractures during load-to-failure testing. The overall strength of the construct is not affected by plate design.

Clinical relevance Microstructural damage or a loss of fixation due to an overly rigid volar plate design may cause malunion or nonunion of fracture fragments and lead to bone-implant instability. *(J Hand Surg Am. 2018;■(■):■−■. Copyright © 2018 by the American Society for Surgery of the Hand. All rights reserved.)*

Key words Distal radius fracture, distal radius plating, volar locking plate, wrist biomechanics, wrist fracture.

*From the *Department of Orthopaedics and Rehabilitation; the †Department of Mechanical Engineering; the ‡Center for Biomedical Engineering; the §Department of Civil Engineering; and the ‖Department of Internal Medicine, University of New Mexico, Albuquerque, NM.*

Received for publication September 17, 2016; accepted in revised form December 20, 2017.

Implants were received from Acumed and Skeletal Dynamics through their research grant mechanism.

Corresponding author: Christina Salas, PhD, Department of Orthopaedics and Rehabilitation, MSC10 5600, 1 University of New Mexico, Albuquerque, NM 87131; e-mail: chrsalas@salud.unm.edu.

0363-5023/18/■ ■-0001$36.00/0
https://doi.org/10.1016/j.jhsa.2017.12.019

Volar locked plating of the distal radius allows for positioning of the plate on the volar cortex of the radius while supporting the distal bone fragments containing the lunate and scaphoid facets. This technology has been evaluated biomechanically focusing on differences compared with dorsally placed plating systems,[1,2] unlocked volar plate systems,[2] plate design,[3–6] fracture type,[3] use of screws versus pegs,[3,4,7] and the number of locked screws used for fixation.[8–10] These studies have independently found that the locked volar plating systems provide sufficient stiffness and strength for use in the treatment of extra-articular and intra-articular distal radius fractures with and without dorsal comminution. To our knowledge, no studies have compared dual-head with single-head, 2-column volar plate designs. In addition, although many studies subject their specimens to cyclic testing before loading the constructs to failure, none have evaluated the effects that low load cyclic testing has on the overall stiffness and strength of the bone-implant constructs.

In this study, we biomechanically evaluated 2 commonly used 2-column plating systems—the Geminus standard, 4-hole volar distal radius plate (Skeletal Dynamics LLC, Miami, FL) and the Acu-Loc2 standard, 3-hole volar distal radius plate (Acumed LLC, Hillsboro, OR). The Geminus plate uses a dual-head design for independent 2-tier scaffolding of the lunate and scaphoid facets. The Acu-Loc2 uses a single-head design for enhanced ulnar buttressing. We chose the Acumed plate because it is one of the most used and heavily cited plates across the United States. We chose the Skeletal Dynamics plate because it has a unique plate design with screw trajectories that claim to be more stable than previous screw trajectory designs. Our evaluation included quantifying the microstructural damage in each bone-implant construct under cyclic loading. "Damage" is an engineering term defining a period between a state of material perfection and the onset of crack initiation. Clinically, it represents a loss of fixation due to microstructural breakdown and can be indirectly measured as a reduction in stiffness of the bone-implant construct, normalized by the cross-sectional area and length of the bone. We examined how this damage affects construct stiffness and strength in subsequent ramped load-to-failure tests simulating a fall on an outstretched hand. Lastly, we evaluated patterns of failure in each bone-implant construct.

MATERIALS AND METHODS

Specimen preparation

Ten matched pairs (n = 20) of fresh-frozen, cadaveric hands with forearms were used in this study. We based our sample sizes on Rausch et al's[6] estimates for stiffness (86 ± 32 vs 159 ± 40) and using a 2-sample *t* test, which should be conservative. With a planned sample size of 10 and these means and standard deviations, we expected statistical power to be >95% with 2-sided alpha equal to 0.05. Specimens were thawed to room temperature and scanned using a Philips Brilliance 64-slice CT scanner (Cleveland, OH) for 3D model development and morphometric measures. Each distal radius was segmented from reconstructed CT dicom data using the Materialise Interactive Medical Image Control System (Materialise, Plymouth, MI) (Fig. 1A). In the axial view, we scrolled proximally 1.5 cm from the distal articular surface of the segmented bone and used the Materialise Interactive Medical Image Control System area measurement system to determine the cross-sectional area at the site of the simulated fracture for each radius (Fig. 1B). These values were used in subsequent damage calculations.

Distal radii were surgically removed from the forearm and sectioned 140 mm proximal to the distal articular surface. An AO type 23-A3.2 extra-articular fracture was simulated by a 1 cm dorsal wedge osteotomy created 1.5 cm proximal to the distal articular surface.[4] Specimens were randomized to 2 groups: group I specimens were treated using a Geminus volar distal radius plate (n = 10); group II specimens (contralateral limbs from specimens in group I) were treated using an Acu-Loc2 volar distal radius plate (n = 10). Three 3.5-mm nonlocking cortical screws secured the plates to the shaft through 2 holes (the 2 most distal shaft holes in group I; both holes in group II) and an oblong gliding hole. Seven 2.3-mm threaded locking pegs were used to secure the plates to the distal fragment.

Mechanical testing

Mechanical testing was performed under cyclic and ramped axial loading conditions using a servohydraulic test frame (Model 858, MTS Systems, Eden Prairie, MN) and 15 kN load cell. The radial shaft was mounted in line with the machine actuator. Load was applied through a custom fixture mounted to the load cell through an angle vise. The fixture ensured a load ratio of 60/40 through the scaphoid and lunate facets to replicate physiologic boundary

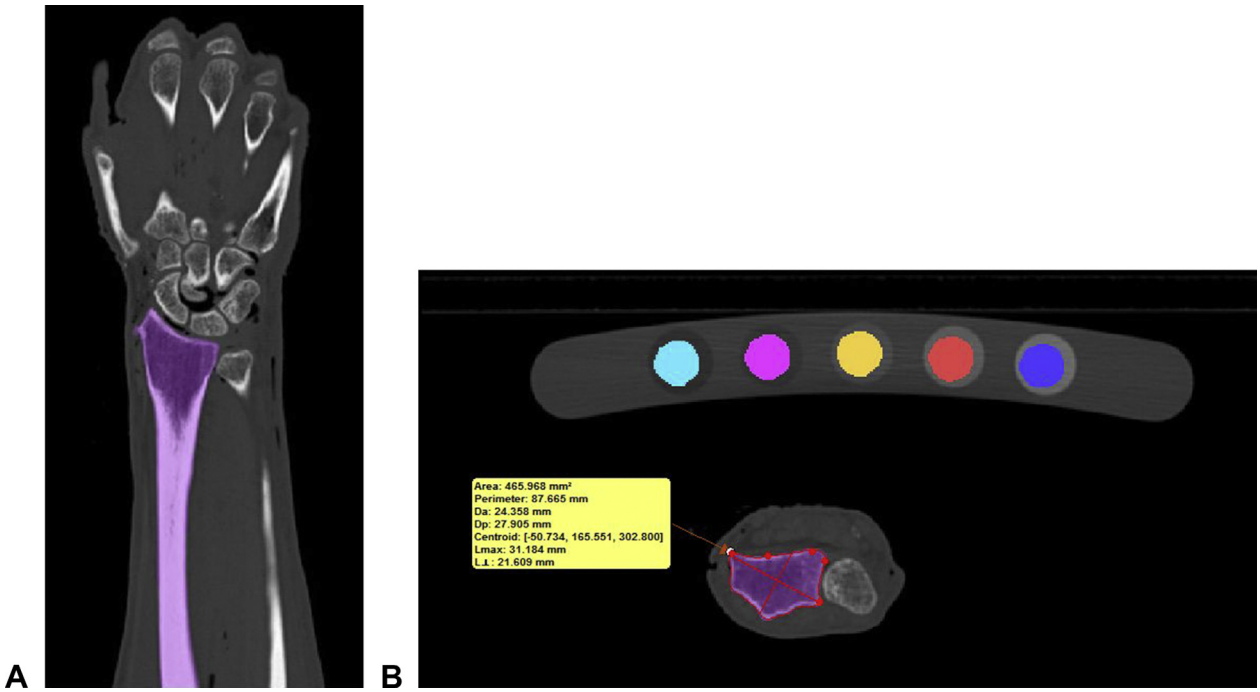

FIGURE 1: **A** Anteroposterior view of the hand and forearm showing the distal radius bone segmentation (purple) using the Materialise Interactive Medical Image Control System (MIMICS) software. **B** Axial view of the wrist showing a 2D slice of the distal radius bone (purple) at the location of simulated fracture. MIMICS measurement tools were used to calculate the cross-sectional area of the bone at this location, for use in subsequent damage calculations.

conditions.[11,12] The vise allowed for adjustment of the angle of the scaphoid/lunate contact points corresponding with geometrical differences in the radii (Fig. 2). Specimens were preloaded to 50 N, held for 30 seconds, and sinusoidally compressed with 50−250 N, at a rate of 1 Hz for 5,000 cycles to simulate a 6-month healing period. This load range was selected based on studies suggesting that forces during light active motion of the wrist range from 100 to 250 N.[13,14] During cyclic testing, the machine was halted every 500 cycles to obtain x-rays for post hoc failure analysis (Hologic Fluoroscan Premier Mini C-arm, Marlborough, MA). Bone-implant constructs that had not failed during cyclic loading were unloaded, held for 30 seconds, and subject to a ramped load to failure at 1 mm/s simulating a fall on an outstretched hand. A Canon EOS Rebel T5i camera (Canon, Tokyo, Japan) set in continuous mode was used for capturing the failure event during load-to-failure tests.

Damage (D; Equation 1) was calculated using the effective modulus of elasticity (E; Equation 2) of the bone-implant constructs from hysteresis data at every 500th cycle.[15] The data were normalized by the effective modulus at cycle 5. This cycle was selected based on published data showing that settling of the bone and implant has occurred by the third cycle.[3]

$$D = 1 - \left[\frac{E_{\text{final}}}{E_{\text{initial}}}\right] \quad (1)$$

where E_{final} is the effective modulus at every 500th cycle and E_{initial} is the effective modulus at cycle 5.

$$E = \frac{PL}{A\Delta} \quad (2)$$

where P is the measured load (N), L is the length of distal radius (0.140 m), A is the cross-sectional area of distal radius at the location of fracture (measured using 3D models from CT scans) (m^2), and Δ is the displacement of bone as measured by the actuator (m).

Failure during cyclic loading was defined as catastrophic fracture of the bone or a decrease in the effective modulus (or stiffness) of greater than 90%. Stiffness and ultimate load data from ramped load-to-failure tests are reported. Experimental test data were analyzed with a custom computer code to evaluate load-displacement hysteresis data and to calculate damage using the Matlab technical computing software (Mathworks, Natick, MA). A 2-tailed, matched-paired t test was used to determine statistical significance ($P < .05$) between groups I and II for stiffness and ultimate load data during ramped load-to-failure testing, respectively.

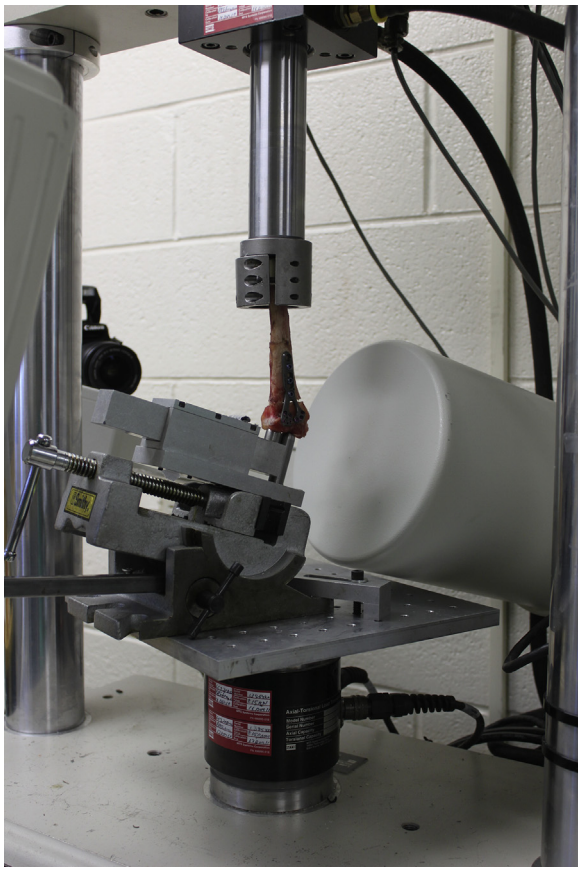

FIGURE 2: Experimental testing fixture showing radial shaft mounted to the load frame actuator. The scaphoid/lunate load applicator is mounted to an angle vise to adjust contact angle to achieve 60/40 load distribution across the distal articular surface. A mini C-arm is positioned to obtain intracyclic x-ray images for failure analysis. A digital camera is positioned to capture failure during ramped loading.

RESULTS

Damage analysis

Group II specimens experienced greater damage (loss of fixation) under cyclic loading conditions than group I specimens (0.78 ± 0.11 and 0.66 ± 0.10, respectively). Figure 3A shows a representative example of the force-displacement hysteresis curves for one specimen in each group with hysteresis data plotted at every 500th cycle. A reduction in stiffness due to microstructural damage is noted by an increase in displacement under constant load. Figure 3B shows a representative example of the damage evolution for one specimen in each group, over the 5,000-cycle test period. Most of the damage accumulation occurred during the first 2,000 cycles of testing for both groups. One specimen in group II experienced volar lunate facet fracture during cyclic loading and was excluded from load-to-failure tests. Thus, the matched pair for this specimen was also eliminated from group I data analysis for load-to-failure tests.

Load to failure

Stiffness for group I (n = 9) and group II (n = 9) specimens was 481.47 ± 161.37 and 337.90 ± 112.04 N/mm, respectively (95% confidence interval [−22.04, 309.17]). Ultimate force at failure in group I and group II specimens was 1,268.50 ± 307.69 and 1,025.63 ± 496.45 N, respectively (95% confidence interval [−235.72, 721.47]).

Patterns of failure

Specimens failed by distal fragment collapse leading to plate bending (group I, n = 6/10; group II, n = 2/10) and fracture of the lunate facet (group I, n = 4/10; group II, n = 8/10) (Fig. 4).

DISCUSSION

In this study, we evaluated 2-tiered (group I) and buttress (group II) type, 2-column volar distal radius plates under cyclic and ramped load-to-failure conditions. We found that the 2-tiered head design limited microstructural damage during low-load cyclic testing. Based on a pattern of failure analysis, it is likely that the damage induced during cyclic loading occurred at the lunate facet fragment in both groups, but was more prevalent in group II. As described in the surgical technique guide for each implant, group I plates have multiplanar screws that are distributed evenly to maximize subchondral bone support and group II plates have parallel screws organized into a proximal and distal row with 2 diverging screws into the radial styloid to maximize screw number. We hypothesize that a mismatch between bone and plate/screw material properties coupled with a rigid buttress design in group II plates may have induced damage to the lower strength bone in the lunate facet region. Slight flexion of the plates was observable in group I specimens during cyclic loading. It is possible that the 2-head design limited extreme plate/screw rigidity that can lead to high stress concentrations at the bone-screw interface. To more accurately determine the cause of the damage to group I and group II specimens, an advanced computational finite element analysis of the stress at the bone-screw interface is necessary. Although group II specimens experienced a greater amount of damage during the 5,000-cycle loading period, it is important to note that the damage did not affect overall construct strength as indicated by a minimal difference in failure strength between the groups (1,268.50 ± 307.69 and 1,025.63 ± 496.45 N, respectively).

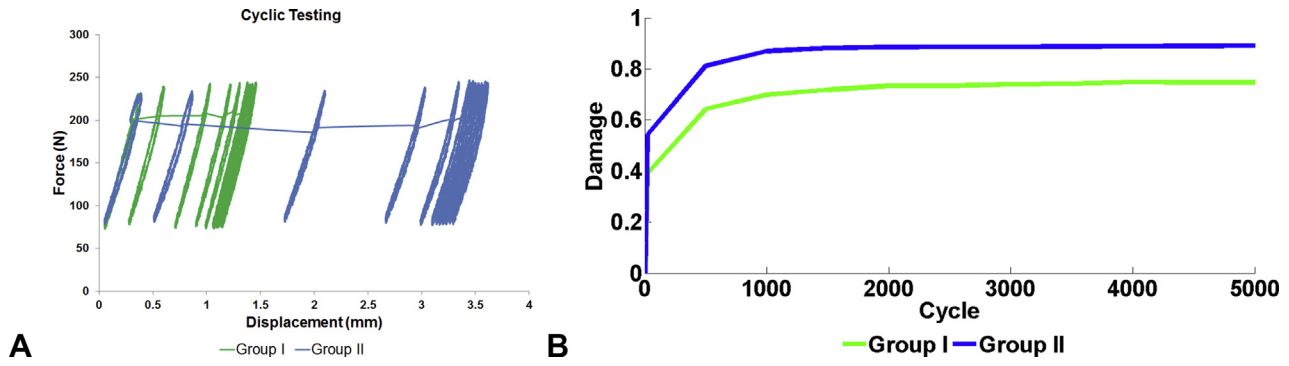

FIGURE 3: **A** Representative force-displacement hysteresis curves of a single specimen from group I and contralateral limb in group II. A reduction in stiffness of each specimen is noted by the increase in displacement under constant loading. Note that the group II specimen has a greater increase in displacement. **B** Representative damage plots of the same 2 specimens over the 5,000-cycle test period. Much of the damage in each specimen accumulated within the first 1,000 cycles with little damage progression after that period.

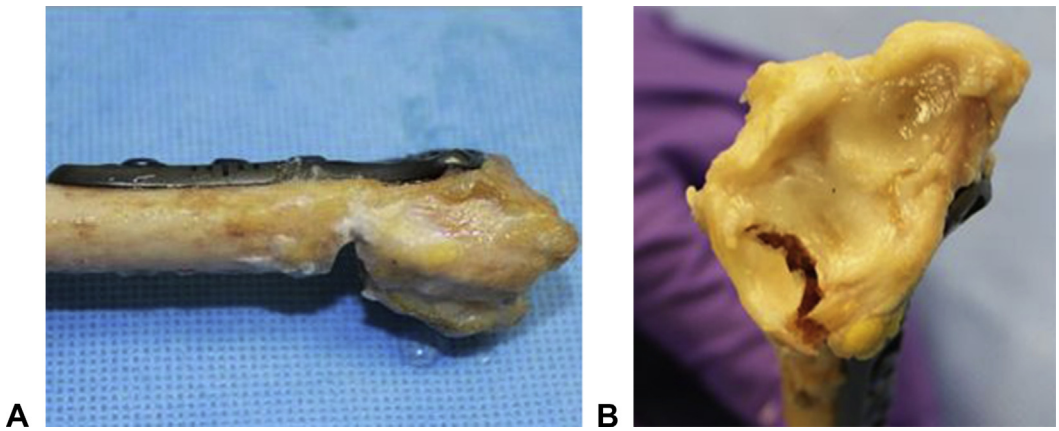

FIGURE 4: Representative images of the failed specimens showing **A** distal fragment collapse leading to plate bending (group I, n = 6/10; group II, n = 2/9), and **B** fracture of the lunate facet (group I, n = 4/10; group II, n = 8/9).

Our study has several strengths. First, this matched, paired study allowed us to compare the 2 plate designs on specimens from the same donor. This limited variability in tissue quality commonly associated with cadaver studies. Second, we simulated the lunate/scaphoid load distribution based on proven physiologic measures. This allowed us to isolate failure patterns by the facet region. Lastly, by normalizing the effective modulus by the cross-sectional area and standardizing the distal radius length, we better captured the level of damage experienced by each specimen.

Our study also has a few limitations. We used cadaveric specimens for this study, so we are unable to simulate healing. It is likely that the effects of healing may offset the effects of the material property mismatch. This study provides a worst-case scenario baseline analysis of the 2 constructs in the closest *in vitro* situation possible—a matched, paired cadaver model. By eliminating healing as a variable, we can focus only on the potential weaknesses and strengths of each construct over time equivalent to the time in which we expect fracture healing to occur. In addition, dorsal comminution with no bone graft/filler simulates the most unstable scenario. It is likely that performance may differ with interposed material. Furthermore, it is unlikely that all distal fragment screws will be used and for the distal fragment to be undamaged. We modeled this fracture/fixation type after previously published articles in this journal.[3,4] Using all available screw holes in the distal fragment of each plate allowed for the most unbiased comparison of the 2 plate designs and eliminated variability in technique for fragment reduction. A future study with multiple bone fragments may be warranted to further evaluate the 2 plate designs and other 2-column plating systems. Lastly, it is important to note that we were unable to draw conclusions as to the statistical significance of our load-to-failure data. Our prestudy power analysis indicated that we

needed 10 specimens to determine significance. Unfortunately, one of our specimens failed catastrophically during damage determination with cyclic testing. We eliminated it and its matched pair from load-to-failure analysis, which brought our sample size to 9. A post hoc analysis of our collected data showed that a sample size of 10 would have enabled significance determination. In fact, assuming that the means and standard deviations of data remained similar for both groups, group I specimens were stiffer than group II specimens under load-to-failure conditions.

Our study design was modeled after that of Dahl et al,[4] who evaluated 8 traditional volar plate designs under cyclic loading followed by ramped load to failure using fourth-generation synthetic bone models. They found that bone-implant stiffness ranged from approximately 200 to 350 N/mm after 6,000 cycles of loading in 2,000-cycle increments of 100, 200, and 300 N. Our stiffness results compare favorably with this study. We found that bone-implant stiffness averaged 481 and 348 N/mm, respectively, after cyclic loading up to 250 N for 5,000 cycles. Stiffness results of our testing also compare moderately with those of Wall et al,[16] who found that fixed-angle volar plates with bicortical screws had a stiffness of 230 N/mm after 1,000 cycles of loading up to 250 N. That study used foam bone models of the distal radius meant to simulate osteoporotic bone, and thus, it is expected that their stiffness values would be slightly less than our findings on cadaver specimens with an average *T*-score of −0.22, indicating normal bone density.

It is important to note that, although this study is validated by comparison of stiffness data with previous studies on a similar topic, this study is unique in that it quantifies the microstructural damage occurring in the bone during cyclic loading. This information may provide insight into the reasons for malunion or nonunion in some locked plate designs. In addition, it may inform implant companies on designs of future volar locking distal radius plates such that the geometry can provide adequate stability without overstiffening or notable rigidity that may lead to microstructural failure of the bone at the bone-screw interface.

ACKNOWLEDGMENTS

We thank Sahar Freedman for providing technical assistance with manuscript editing. Special thanks to Acumed and Skeletal Dynamics for providing the locked volar plates, screws, and surgical instrument trays used in this study through their respective research grant-funding mechanisms. This research is supported in part by the National Institutes of Health through the University of New Mexico Clinical and Translational Science Center (CTSC Grant Number UL1TR001449).

REFERENCES

1. Kandemir U, Matityahu A, Desai R, Puttlitz C. Does a volar locked plate provide equivalent stability as a dorsal nonlocking plate in a dorsally comminuted distal radius fracture? A biomechanical study. *J Orthop Trauma*. 2008;22(9):605−610.
2. Willis AA, Kutsumi K, Zobitz ME, Cooney WP III. Internal fixation of dorsally displaced fractures of the distal part of the radius. A biomechanical analysis of volar plate fracture stability. *J Bone Joint Surg Am*. 2006;88(11):2411−2417.
3. Koh S, Morris RP, Patterson RM, Kearney JP, Buford WL Jr, Viegas SF. Volar fixation for dorsally angulated extra-articular fractures of the distal radius: a biomechanical study. *J Hand Surg Am*. 2006;31(5):771−779.
4. Dahl WJ, Nassab PF, Burgess KM, et al. Biomechanical properties of fixed-angle volar distal radius plates under dynamic loading. *J Hand Surg Am*. 2012;37(7):1381−1387.
5. Kamei S, Osada D, Tamai K, et al. Stability of volar locked plate systems for AO type C3 fractures of the distal radius: biomechanical study in a cadaveric model. *J Orthop Sci*. 2010;15(3):357−364.
6. Rausch S, Klos K, Stephan H, et al. Evaluation of polyaxial angle-stable volar plate in a distal radius C-fracture model—a biomechanical study. *Injury*. 2011;42(11):1248−1252.
7. Mehling I, Klitscher D, Mehling AP, et al. Volar fixed-angle plating of distal radius fractures: screws versus pegs—a biomechanical study in a cadaveric model. *J Orthop Trauma*. 2012;26(7):395−401.
8. Moss DP, Means KR Jr, Parks BG, Forthman CL. A biomechanical comparison of volar locked plating of intra-articular distal radius fractures: use of 4 versus 7 screws for distal fixation. *J Hand Surg Am*. 2011;36(12):1907−1911.
9. Sokol SC, Amanatullah DF, Curtiss S, Szabo RM. Biomechanical properties of volar hybrid and locked plate fixation in distal radius fractures. *J Hand Surg Am*. 2011;36(4):591−597.
10. Crosby SN, Fletcher ND, Yap ER, Lee DH. The mechanical stability of extra-articular distal radius fractures with respect to the number of screws securing the distal fragment. *J Hand Surg Am*. 2013;38(6):1097−1105.
11. Majima M, Horii E, Matsuki H, Hirata H, Genda E. Load transmission through the wrist in the extended position. *J Hand Surg Am*. 2008;33(2):182−188.
12. Edwards WB, Troy KL. Simulating distal radius fracture strength using biomechanical tests: a modeling study examining the influence of boundary conditions. *J Biomech Eng*. 2011;133(11):114501.
13. Rikli DA, Honigmann P, Babst R, Cristalli A, Morlock MM, Mittlmeier T. Intra-articular pressure measurement in the radio-ulnocarpal joint using a novel sensor: *in vitro* and *in vivo* results. *J Hand Surg Am*. 2007;32(1):67−75.
14. Horii E, Garcia-Elias M, Bishop AT, Cooney WP, Linscheid RL, Chao EY. Effect on force transmission across the carpus in procedures used to treat Kienböck's disease. *J Hand Surg Am*. 1990;15(3):393−400.
15. Lemaitre J, Chaboche J-L. *Mechanics of Solid Materials*. 1st ed. Cambridge, UK: Cambridge University Press; 1990.
16. Wall LB, Brodt MD, Silva MJ, Boyer MI, Calfee RP. The effect of screw length on stability of simulated osteoporotic distal radius fractures fixed with volar locking plates. *J Hand Surg Am*. 2012;37(3):446−453.